applied sciences

MDPI

Article

Dynamic Corrosion Test Using $LiNO_3$ Containing Molten Salt for CSP Applications

Angel G. Fernández [1,2,*], Belén Muñoz-Sánchez [3], Javier Nieto-Maestre [3] and Luisa F. Cabeza [2]

1 Energy Development Center, University of Antofagasta, Av. Universidad de Antofagasta s/n, Antofagasta 02800, Chile
2 GREiA Research Group, Universitat de Lleida, Pere de Cabrera s/n, 25001 Lleida, Spain; luisaf.cabeza@udl.cat
3 TECNALIA, Basque Research and Technology Alliance (BRTA), Mikeletegi Pasealekua, 2, 20009 San Sebastián, Guipúzcoa, Spain; belen1984iq@gmail.com (B.M.-S.); javier.nieto@tecnalia.com (J.N.-M.)
* Correspondence: angel.fernandez@udl.cat; Tel.: +34-973-003515

Received: 18 May 2020; Accepted: 19 June 2020; Published: 23 June 2020

Featured Application: Concentrating solar power technology, dynamic corrosion assessment on TES materials at high temperature.

Abstract: Low melting point thermal energy storage (TES) materials have been proposed in the last years to reduce the storage cost in concentrating solar power (CSP) technology. One of the most interesting additive due to the enhancement in thermal properties is lithium nitrate. However, there is a lack of dynamic corrosion tests to simulate real operation conditions in CSP plants. In this work, we present a dynamic reactor set up where a mixture of 30 wt.% $LiNO_3$ + 57 wt.% KNO_3 + 13 wt.%. $NaNO_3$ is moved through a mechanical stirrer obtaining a lineal speed of 0.30 m/s. A commercial carbon steel A516 was tested as container material at 390 °C during 1000 h. Fe_2O_3 and Fe_3O_4 were obtained as the main corrosion products by scanning electron microscopy (SEM) and x-ray diffraction (XRD) with a metallographic corrosion rate of 0.015 mm/year.

Keywords: dynamic corrosion; thermal energy storage; concentrated solar power; lithium nitrate salts

1. Introduction

According to the International Energy Agency (IEA) [1], concentrated solar power (CSP) plant capacity is expected to grow 87% (4.3 GW) over the forecast period of 2018–2023, which is a 32% increase compared to 2012–2017. China leads the production with 1.9 GW, followed by 1 GW from projects that receive multilateral development bank support in Morocco and South Africa, 1 GW in the Middle East, and 300 MW each in Australia and Chile.

Spain and the United States, the two countries with the most installed capacity, are not expected to commission projects over the forecast period. Therefore, China is expected to overtake the United States to have the second-largest CSP capacity installed by 2023.

Recent auction results indicate significant cost-reduction potential. But technology risk, restricted access to financing, long project lead-time, and market designs that do not value thermal energy storage (TES) continue to challenge CSP deployment [1].

The cost reduction in CSP technology has been one of the main objectives, especially in the storage block. In this direction, different additives have been proposed in order to improve the thermal properties in the solar salt (60 wt.% $NaNO_3$ + 40 wt.% KNO_3), as $NaNO_2$, $Ca(NO_3)_2$ and $LiNO_3$ [2–6]. Table 1 shows the main thermal properties obtained with these additions compared to solar salt.

Table 1. Thermal properties obtained in molten salts with $LiNO_3/Ca(NO_3)_2$ additions compared with solar salt.

Molten Salt (wt.%)	Melting Point (°C)	Thermal Stability (°C)	Heat Capacity (J/g °C)	Viscosity at 250 °C (cP)	Ref.
$60NaNO_3$-$40KNO_3$	221	589	1.54	5.51	[2]
30 $LiNO_3$-10 $Ca(NO_3)_2$-60 KNO_3	132	567	1.40	5.72	[3]
10 $LiNO_3$-10 $Ca(NO_3)_2$-60 KNO_3-20 $NaNO_3$	132	580	1.55	5.78	[4,5]
30 $LiNO_3$-57 KNO_3-13 $NaNO_3$	123	595	1.74	5.65	[6]

Since $NaNO_2$ needs to use an inert atmosphere to avoid the oxidation of $NaNO_2$ to $NaNO_3$ as well as the early thermal decomposition of $Ca(NO_3)_2$ mixture beyond 520 °C [7], $LiNO_3$ has been proposed as one of the main interesting additives to TES materials based on nitrate salts.

As shown in Table 1, the addition of $LiNO_3$ could reduce the melting points of these molten salt mixtures to 130 °C obtaining a work temperature range around 465 °C [6]. This reduction in the melting point temperature can improve the parasitic consumption due to freezing protection systems, also in addition to the effect of increasing the current field temperature limitation and the impact on plant capacity factor, therefore, an interesting cost reduction could be obtained in the CSP plant economic balance related with the storage block. The thermal properties obtained by adding $LiNO_3$ to solar salt have been studied by several researchers [3,8–10], including also the corrosive behavior of these mixtures in commercial alloys at the storage target temperatures in parabolic trough and central tower power plants, 390 °C and 550 °C, respectively. Table 2 shows the main results obtained in carbon and stainless steels.

Table 2. Corrosion rates obtained in $LiNO_3$ ternary nitrate mixture.

Molten Salt (wt.%)	Steel	Temperature (°C)	Time (hours)	Corrosion Rate (mm/year)	Ref.
20 $LiNO_3$ + 52 KNO_3 + 28 $NaNO_3$	A1	390	2000	0.040	[11]
30 $LiNO_3$ + 57 KNO_3 + 13 $NaNO_3$	SB450	550	1000	0.150	[12]
30 $LiNO_3$ + 57 KNO_3 + 13 $NaNO_3$	T22 (2%Cr)	550	1000	0.130	[12]
30 $LiNO_3$ + 57 KNO_3 + 13 $NaNO_3$	T91 (9%Cr)	550	1000	0.013	[12]
30 $LiNO_3$ + 57 KNO_3 + 13 $NaNO_3$	X20 (12%Cr)	550	1000	0.005	[12]
30 $LiNO_3$ + 57 KNO_3 + 13 $NaNO_3$	AISI304	550	1000	0.004	[13]
30 $LiNO_3$ + 57 KNO_3 + 13 $NaNO_3$	In702	550	1000	0.002	[13]
30 wt.% $LiNO_3$ + 57 wt.% KNO_3 + 13 wt.% $NaNO_3$	OCT	550	1000	0.006	[13]

The selection of the materials for tanks, piping and other components is made taking into account the potential corrosion and the operation temperature. In general, stainless steel (AISI 347) is selected for zones where the salt temperature could exceed 400 °C, whereas the rest of pipes and tanks are made of carbon steel (A516). Nevertheless, there is a lack of knowledge about the compatibility of molten salts with common container materials under dynamic conditions.

Corrosion is expected to be enhanced in dynamic conditions, due to continuous renewal of the molten salt layer in contact with the metal surface, or the erosion of the passivating oxide layer. In this direction, Fernandez et al. [14] reported the higher corrosion rate comparing dynamic and static set ups, using a molten salt pilot plant with a $LiNO_3$ ternary molten salt in contact with AISI 316, using the composition proposed in this study. The major corrosion test reported in the literature are focused on the study of the effect of the chloride content as well as the impurity influence in this process, using the binary solar salt (60 wt.% $NaNO_3$ + 40 wt.% KNO_3).

García-Martín et al. [15] performed a corrosion test under dynamic conditions using analytical grade solar salt (164 ppm Cl^-) in a closed loop during 100 h. This research showed a notable increase

of corrosion in dynamic conditions. However, the experiment was very short to be compared with other studies.

In the present study, a dynamic corrosion set up is proposed in order to simulate the real testing conditions in CSP plants, using a dynamic corrosion reactor with a mechanical stirrer. Corrosion test was carried out at 390 °C in A516 immersed in the ternary mixture composed by 30 wt.% $LiNO_3$ + 57 wt.% KNO3 + 13 wt.% $NaNO_3$ during 1000 h.

2. Methodology

Molten salts mixtures used for this research are KNO_3, $NaNO_3$ (SQM refined 99%, Antofagasta, Chile) and $LiNO_3$ (Todini 99%, Milan, Italy). Molten salts were dried in an oven at 100 °C for 1 h before the preparation of the ternary salt and a stepwise heating was applied to reduce the water content and obtain a homogeneous mixture. Three samples of carbon steel A516 were prepared from bulk materials with dimensions of 25 × 10 × 2 mm, providing a hole for hanging in the sample holder. The samples were polished using abrasive papers (SiC) with different granulometry (from #320 to #1200) to remove any existing oxide layer before the corrosion test.

As it was mentioned before, A516 was the selected steel since it presents a suitable commercial solution for CSP plants and it has been used in parabolic trough solar plants at storage temperatures below 400 °C. Its composition is showed in Table 3.

Table 3. Chemical composition of carbon steel A516.

Alloy	**Weight (%)**					
A516	Si	Mn	P	C	S	Fe
	0.25	1.1	0.025	0.29	0.03	Balance

An autoclave of 4 L of volume was employed to test the corrosion induced by the salts under dynamic conditions. The autoclave components in contact with the molten salt, as well as the stirrer and the thermocouple sheath were made of Hastelloy C276.

The stirrer was placed at the end of a hollow tube, employed to cool the stirrer down with water during operation. An amount of 2.7 kg of the lithium nitrate mixture was charged on the autoclave (Figure 1 left) and A516 coupons were placed concentrically to the mixer on a rack specially designed to this experiment (Figure 1, right).

With this configuration, the molten salt flowed over the specimens at the same speed. The angular velocity of the mixer was 1250 rpm, which is equivalent to a lineal speed of 0.30 m/s.

Figure 1. Autoclave filled with the lithium ternary molten salt (**left**) and detail of the rack with alloys specimens and the mixer (**right**).

The temperature was set up at 150 °C for two hours to achieve the complete melting of the salt and then it was increased slowly until the testing temperature of 390 °C was reached.

Test coupons were removed from the molten salt at 200, 600 and 1000 h, cooled slowly and cleaned with hot distilled water. The formula (Equation (1)) used to calculate the mass gain over time is:

$$\frac{\Delta m}{S_0} = \frac{m_f - m_i}{S_0} \quad (1)$$

where m_i is the initial mass of the specimen, m_f is the mass of the same at time t, and S_0 is the initial area of the specimen. Coupons were weighed in a precision balance (±0.0001 g) AG135 from Mettler-Toledo.

Morphology and elemental composition of the exposed surfaces and their cross sections were inspected by SEM, model JEOL JSM-7500F, operated in high vacuum mode at 20 keV equipped with a backscattered electron detector, used for the microstructural analysis, and coupled to energy dispersive X-ray spectrometer (EDS) analyzer with a recommended working distance of around 10 mm. The top surfaces were inspected without further surface manipulation. For cross section studies, coupons were mounted in a polymer resin prepared by mixing Remet Hardrock 554 resin and the hardener catalyst, in 2:1 proportion. After the resin cured (24 h at room temperature), the samples were grinded and polished using SiC for a proper preparation.

Crystallographic phase composition was determined by X-Ray diffraction using a PANalytical X'Pert PRO MDP and powder diffraction database. For XRD analysis, $\theta/2\theta$ Bragg-Brentano powder diffractometer of 240 millimeters of radius was used with a copper anode with kα radiation of λ = 1.5418 Å. Tests were carried out using a grazing incidence from 5 to 120° with a step size of 0.017° and a measuring time of 50 s per step.

3. Results and Discussion

Table 4 shows the weight increments divided by the surface area of the samples. In the case of A516 carbon steel the weight increases between 200 h and 600 h and remains constant at times higher than 600 h.

Table 4. Weight change per surface area of the samples removed after 200 h, 600 h and 1000 h exposure in the corrosion test at 390 °C.

Alloy	Δm/S (mg·cm^{-2})		
A516	200 h	600 h	1000 h
	0.2677	0.3231	0.3155

Superficial SEM characterization of the surface of the samples at 200 h and 600 h was performed. In the case of A516 (Figure 2), the image at 200 h (left) shows a uniform corrosion layer with a small area (spectrum 1) without corrosion, detecting the base material in the EDS analysis.

EDS (wt.%)	O	Mg	Si	Mn	Fe
Spot 1	5.50	-	0.45	1.38	89.50
Spot 2	33.60	16.57	0.54	0.68	43.06
Spot 3	36.80	11.81	0.67	0.69	40.67

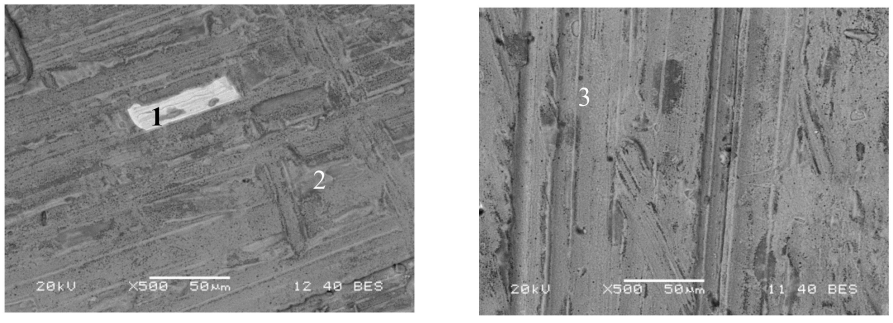

Figure 2. Backscattered surface image CS A516 at 200 h (**Left**) and 600 h (**Right**).

The corrosion layer is mainly composed by Fe-O with magnesium content as an active impurity from the salt [16]. Cross sectional study was analyzed at the end of the test (1000 h) and it is shown in Figure 3.

EDS (wt.%)	O	Mg	Si	Mn	Fe
A516	32.97	9.71	0.64	0.90	46.47

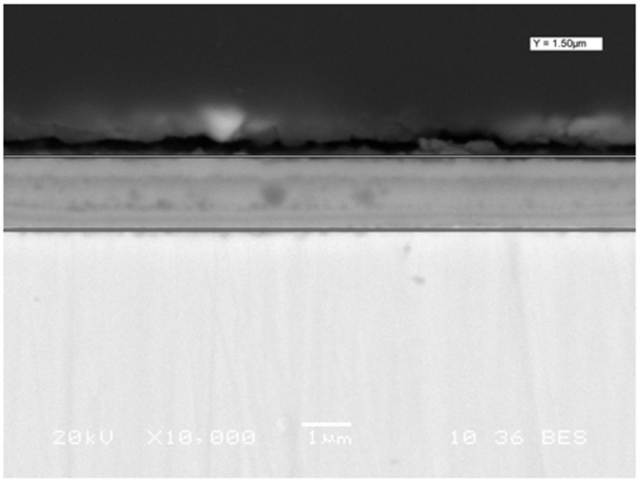

Figure 3. Backscattered cross section study in corrosion layer of A516 at 1000 h of immersion in $LiNO_3$ ternary molten salt at 390 °C.

The corrosion layer thickness was measured from Figure 3, taken at different distances from the edge of the sample (2 mm, 6 mm, 10 mm, 14 mm and 18 mm). The average thickness was considered as the layer thickness.

This procedure was also repeated at the intermediate measure times. Table 5 shows the thickness of A516 at different times (200 h, 600 h and 1000 h). In average, the corrosion layer thickness increases until 600 h and remains constant between 600 and 1000 h.

Table 5. Thickness of the corrosion layer at different times in µm.

Distance	Thickness (µm) at 200 h	Thickness (µm) at 600 h	Thickness (µm) at 1000 h
2 mm	1.40	1.74	1.5
6 mm	1.52	1.72	1.42
10 mm	1.50	1.56	1.74
14 mm	0.96	1.80	1.88
18 mm	1.04	1.80	1.98
ave	1.28	1.72	1.70
S_{n-1}	0.26	0.10	0.24

The velocity of corrosion is $1.70 \cdot 10^{-3}$ µm/h that corresponds to 0.015 mm/year. Attending to the recommendations of Ghali et al. [17] (Table 6), this material would be recommended for long term service. However, additional corrosion test with longer exposure times are recommended.

The profile of compositions was analyzed by SEM. Figure 4 shows the concentration of Fe (blue) and O (red) as a function of the distance from the surface of the steel.

Three zones can be observed in the pictures. Zone I (0.2 µm) contains higher amount of oxygen, since Fe diffusion is lower in this outer zone. Zone II shows similar concentrations of Fe and oxygen. It is possible that the principal compound in this zone is Fe_2O_3. Zone III shows a different pattern, the content of Fe increases and the oxygen one decreases. This could be due to the evolution of hematite (Fe_2O_3) to magnetite (Fe_3O_4). A clear transition in the gray tonality is detected between Zone II and Zone III in Figure 5 (right).

Table 6. Corrosion rate and their cooperativity in industries. Adapted from [17].

Corrosion Rate (mg/cm^2 year)	Corrosion Rate (mm/year)	Recommendation
>1000	>2	Completely destroyed within days
100 to 999	0.2–1.99	Not recommended for service greater than a month
50 to 99	0.1–0.19	Not recommended for service greater than one year
10 to 49	0.02–0.09	Caution recommended, based on the specific application
0.3 to 9.9	NA	Recommended for long term service
<0.2	NA	Recommended for long term service; no corrosion, other than as a result of surface cleaning, was evidenced

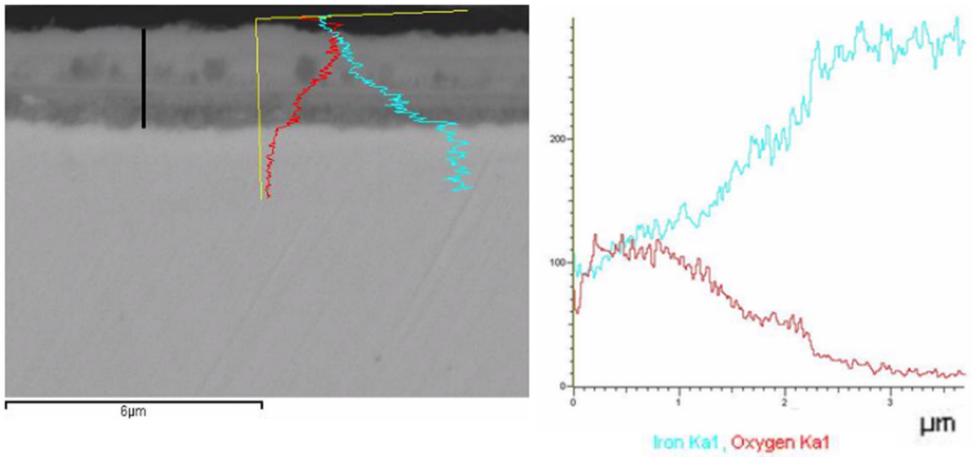

Figure 4. Backscattered SEM picture of the corrosion layer obtained in A516 at 1000 h (**left**) and concentration profile of Fe and O (**right**).

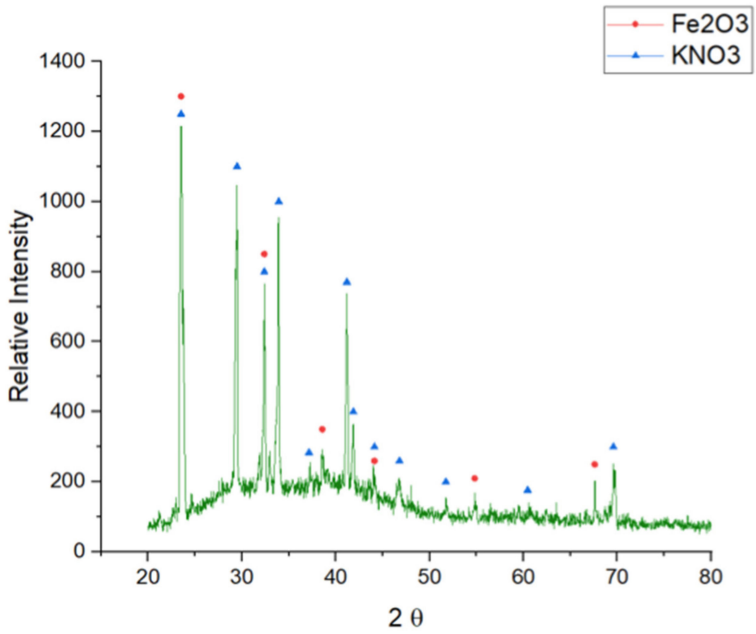

Figure 5. XRD analysis for A516 after 1000 h of immersion in $LiNO_3$ ternary molten salt at 390 °C.

In order to complete the corrosive characterization, a XRD analysis was carried out in the A516 steel at the end of the test (Figure 5).

Hematite (Fe_2O_3) was obtained as the main corrosive impurity detected in the steel surface, generating a non-protective scale in the steel surface.

4. Conclusions

A dynamic corrosion test was performed to evaluate the compatibility of a mixture of nitrate salts containing 30wt.% $LiNO_3$ + 13wt.% $NaNO_3$ + 57wt.% KNO_3 in A516 carbon steel.

The composition profile for A516 corrosion was analyzed in three different zones mapping the content in iron and oxygen, obtaining the presence of magnetite (Fe_3O_4) for the inner layers and hematite (Fe_2O_3) for the outer layers. The thickness variation over the time was also monitorized during the experiment obtaining a metallographic corrosion rate of 0.015 mm/year. This corrosion rate would allow the use of this material for long-term service in CSP plants.

Due to the lack of knowledge about the compatibility of molten salts with common container materials in the literature, this work can contribute to increase the knowledge in dynamic corrosion results using molten salts as thermal energy storage material.

Author Contributions: Conceptualization, A.G.F. and L.F.C.; methodology, J.N.M., B.M.-S., A.G.F. and L.F.C.; lab testing, J.N.-M., B.M.-S.; software, J.N.-M., B.M.-S.; formal analysis, B.M.-S., A.G.F., and L.F.C.; investigation, J.N.-M., A.G.F. and L.F.C.; writing—original draft preparation, A.G.F.; writing—review and editing, L.F.C.; supervision, L.F.C.; project administration, A.G.F.; funding acquisition, A.G.F.. All authors have read and agreed to the published version of the manuscript.

Funding: The authors would like to acknowledge the financial support provided by CONICYT/FONDAP 15110019 "Solar Energy Research Center" SERC-Chile. This work was partially funded by the Ministerio de Ciencia, Innovación y Universidades de España (RTI2018-093849-B-C31- MCIU/AEI/FEDER, UE). This work was partially funded by the Ministerio de Ciencia, Innovación y Universidades-Agencia Estatal de Investigación (AEI) (RED2018-102431-T). This work is partially supported by ICREA under the ICREA Academia programme.

Acknowledgments: The authors would like to thank the Catalan Government for the quality accreditation given to their research group (GREiA 2017 SGR 1537). GREiA is certified agent TECNIO in the category of technology developers from the Government of Catalonia.

Conflicts of Interest: The authors declare no conflicts of interest. The funders had no role in the design of the study; in the collection, analyses, or interpretation of data; in the writing of the manuscript, or in the decision to publish the results.

References

1. Agency, I.E. Renewables 2018: Market Analysis and Forecast from 2018 to 2023. 2018. Available online: https://www.iea.org (accessed on 14 April 2020).
2. Fernandez, A.G.; Lasanta, M.I.; Perez, F.J. Molten Salt Corrosion of Stainless Steels and Low-Cr Steel in CSP Plants. *Oxid. Met.* **2012**, *78*, 329–348. [CrossRef]
3. Fernandez, A.G.; Ushak, S.; Galleguillos, H.; Perez, F.J. Development of new molten salts with $LiNO_3$ and $Ca(NO_3)_2$ for energy storage in CSP plants. *Appl. Energy* **2014**, *119*, 131–140. [CrossRef]
4. Cabeza, L.F.; Gutierrez, A.; Barreneche, C.; Ushak, S.; Fernandez, A.G.; Fernandez, A.I.; Grageda, M. Lithium in thermal energy storage: A state-of-the-art review. *Renew. Sustain. Energy Rev.* **2015**, *42*, 1106–1112. [CrossRef]
5. Fernandez, A.G.; Gomez, J. Thermophysical properties of low cost lithium nitrate salts produced in northern Chile for thermal energy storage. *Renew. Energy* **2017**, *101*, 120–125. [CrossRef]
6. Henriquez, M.; Guerreiro, L.; Fernandez, A.G.; Fuentealba, E. Lithium nitrate purity influence assessment in ternary molten salts as thermal energy storage material for CSP plants. *Renew. Energy* **2020**, *149*, 940–950. [CrossRef]
7. Olivares, R.I. The thermal stability of molten nitrite/nitrates salt for solar thermal energy storage in different atmospheres. *Sol. Energy* **2012**, *86*, 2576–2583. [CrossRef]
8. Wang, T.; Mantha, D.; Reddy, R.G. Thermal stability of the eutectic composition in $LiNO_3$–$NaNO_3$–KNO_3 ternary system used for thermal energy storage. *Sol. Energy Mater. Sol. Cells* **2012**, *100*, 162–168. [CrossRef]
9. Mohammad, M.B.; Brooks, G.; Rhamdhani, M.A. Thermal analysis of molten ternary lithium-sodium-potassium nitrates. *Renew. Energy* **2017**, *104*, 76–87. [CrossRef]

10. Fernandez, A.G.; Gomez, J.; Oro, E.; Kruizenga, A.; Sole, A.; Cabeza, L.F. Mainstreaming commercial CSP systems: A technology review. *Renew. Energy* **2019**, *140*, 152–176. [CrossRef]
11. Fernandez, A.G.; Perez, F.J. Improvement of the corrosion properties in ternary molten nitrate salts for direct energy storage in CSP plants. *Sol. Energy* **2016**, *134*, 468–478. [CrossRef]
12. Cheng, W.J.; Chen, D.J.; Wang, C.J. High temperature corrosion of Cr-Mo steel in molten $LiNO_3$-$NaNO_3$-KNO_3 eutectic salt for thermal energy storage. *Sol. Energy Mater. Sol. Cells* **2015**, *132*, 563–569. [CrossRef]
13. Fernandez, A.G.; Cabeza, L.F. Corrosion Monitoring and Mitigation Techniques on Advanced Thermal Energy Storage Materials for CSP Plants. *Sol. Energy Mater. Sol. Cells* **2019**, *192*, 179–187. [CrossRef]
14. Fernández, A.G.; Henriquez, M.; Mallco, A.; Muñoz-Sánchez, B.; Nieto-Maestre, J. Dynamic corrosion tests comparison: Dynamic reactor vs high temperature pilot plant scale setup for Chilean LiNO3 containing molten salt. In *AIP Conference Proceedings*; AIP Publishing LLC.: Melville, NY, USA, 2018; Volume 2033, p. 090009.
15. García-Martín, G.; Lasanta, M.I.; Encinas-Sanchez, V.; de Miguel, M.T.; Perez, F.J. Evaluation of corrosion resistance of A516 Steel in a molten nitrate salt mixture using a pilot plant facility for application in CSP plants. *Sol. Energy Mater. Sol. Cells* **2017**, *161*, 226–231. [CrossRef]
16. Prieto, C.; Rubio, C.; Ruiz-Cabañas, F.J.; Rodríguez-Sanchez, A.; Fernández, A.I.; Martínez, M.; Oró, E.; Cabeza, L.F. Effect of the impurity magnesium nitrate in the thermal decomposition of the Solar Salt. *Sol. Energy* **2019**, *192*, 186–192. [CrossRef]
17. Ghali, E.; Vedula, S.; Sastri, E.; Elboujdaini, M. *Corrosion Prevention and Protection: Practical Solutions*; J. Wiley Ltd.: Hoboken, NJ, USA, 2007.